Comparison of micromagnetic parameters of the ferromagnetic semiconductors (Ga,Mn)(As,P) and (Ga,Mn)As

N. Tesařová,[1] D. Butkovičová,[1] R. P. Campion,[2] A. W. Rushforth,[2] K. W. Edmonds,[2] P. Wadley,[2] B. L. Gallagher,[2] E. Schmoranzerová,[1] F. Trojánek,[1] P. Malý,[1] P. Motloch,[4] V. Novák,[3] T. Jungwirth,[3,2] and P. Němec[1,*]

[1]*Faculty of Mathematics and Physics, Charles University in Prague, Ke Karlovu 3, 121 16 Prague 2, Czech Republic*

[2]*School of Physics and Astronomy, University of Nottingham, Nottingham NG72RD, United Kingdom*

[3]*Institute of Physics ASCR, v.v.i., Cukrovarnická 10, 16253 Prague 6, Czech Republic*

[4]*University of Chicago, Chicago, Illinois 60637, USA*

(Received 6 May 2014; revised manuscript received 29 September 2014; published 23 October 2014)

We report on the determination of micromagnetic parameters of epilayers of the ferromagnetic semiconductor (Ga,Mn)As, which has an easy axis in the sample plane, and (Ga,Mn)(As,P), which has an easy axis perpendicular to the sample plane. We use an optical analog of ferromagnetic resonance where the laser-pulse-induced precession of magnetization is measured directly in the time domain. By the analysis of a single set of pump-and-probe magneto-optical data, we determined the magnetic anisotropy fields, the spin stiffness, and the Gilbert damping constant in these two materials. We show that incorporation of 10% of phosphorus in (Ga,Mn)As with 6% of manganese leads not only to the expected sign change of the perpendicular-to-plane anisotropy field but also to an increase of the Gilbert damping and to a reduction of the spin stiffness. The observed changes in the micromagnetic parameters upon incorporating P in (Ga,Mn)As are consistent with the reduced hole density, conductivity, and Curie temperature of the (Ga,Mn)(As,P) material. We also show that the apparent magnetization precession damping is stronger for the $n = 1$ spin wave resonance mode than for the $n = 0$ uniform magnetization precession mode.

DOI: 10.1103/PhysRevB.90.155203 PACS number(s): 75.50.Pp, 75.30.Gw, 75.70.−i, 78.20.Ls

I. INTRODUCTION

(Ga,Mn)As is the most widely studied diluted magnetic semiconductor (DMS) with a carrier-mediated ferromagnetism [1]. Investigation of this material system can provide fundamental insight into new physical phenomena that are present also in other types of magnetic materials—like ferromagnetic (FM) metals—where they can be exploited in spintronic applications [2–5]. Moreover, the carrier concentration in DMSs is several orders of magnitude lower than in conventional FM metals, which enables manipulation of magnetization by external stimuli; e.g., by electric [6,7] and optical [8,9] fields. Another remarkable property of this material is a strong sensitivity of the magnetic anisotropy to the epitaxial strain. (Ga,Mn)As epilayers are usually prepared on a GaAs substrate where the growth-induced compressive strain leads to in-plane orientation of the easy axis (EA) for Mn concentrations $\geqslant$2% [10]. However, for certain experiments, e.g., for a visualization of magnetization orientation by the magneto-optical (MO) polar Kerr effect [11–17] or the anomalous Hall effect [12,18], the EA orientation in the direction perpendicular to the sample plane is more suitable. To achieve this, (Ga,Mn)As layers have been grown on relaxed (In,Ga)As buffer layers that introduce a tensile strain in (Ga,Mn)As [11,12,14,16–18]. However, the growth on (In,Ga)As layers can result in a high density of line defects that can lead to high coercivities and a strong pinning of domain walls (DWs) [16,17]. Alternatively, tensile strain and perpendicular-to-plane orientation of the EA can be achieved by the incorporation of small amounts of phosphorus in (Ga,Mn)(As,P) layers [19,20]. In these epilayers, the EA can be in the sample plane for the as-grown material and perpendicular to the plane for fully annealed (Ga,Mn)(As,P) [21]. The possibility of magnetic anisotropy fine tuning by the thermal annealing turns out to be a very favorable property of (Ga,Mn)(As,P) because it enables the preparation of materials with extremely low barriers for magnetization switching [22,23]. Compared to tensile-stained (Ga,Mn)As/(In,Ga)As films, (Ga,Mn)(As,P)/GaAs epilayers show weaker DW pinning, which allows observation of the intrinsic flow regimes of DW propagation [13,15,24].

Preparation of uniform (Ga,Mn)As epilayers with minimized density of unintentional extrinsic defects is a rather challenging task that requires optimized growth and post-growth annealing conditions [25]. Moreover, the subsequent determination of material micromagnetic parameters by the standard characterization techniques, such as ferromagnetic resonance (FMR), is complicated by the fact that these techniques require rather thick films, which may be magnetically inhomogeneous [25,26]. Recently, we have reported the preparation of high-quality (Ga,Mn)As epilayers where the individually optimized synthesis protocols yielded systematic doping trends, which are microscopically well understood [25]. Simultaneously with the optimization of the material synthesis, we developed an optical analog of FMR (optical-FMR) [25], where all micromagnetic parameters of the in-plane (Ga,Mn)As were deduced from a single MO pump-and-probe experiment in which a laser pulse induces precession of magnetization [27,28]. In this method the anisotropy fields are determined from the dependence of the precession frequency on the magnitude and the orientation of the external magnetic field, the Gilbert damping constant is deduced from the damping of the precession signal, and the spin stiffness is obtained from the mutual spacing of the spin wave resonance (SWR) modes observed in the measured MO signal. In this paper we apply this all-optical FMR to (Ga,Mn)(As,P). We demonstrate the applicability of this method also for the

*Corresponding author: nemec@karlov.mff.cuni.cz

determination of micromagnetic parameters in DMS materials with a perpendicular-to-plane orientation of the EA. By this method we show that the incorporation of P in (Ga,Mn)As leads not only to the expected sign change of the perpendicular-to-plane anisotropy field but also to a considerable increase of the Gilbert damping and to a reduction of the spin stiffness. Moreover, we illustrate that the all-optical FMR can be very effectively used not only for an investigation of the uniform magnetization precession but also for a study of SWRs.

II. EXPERIMENTAL

In our previous paper we reported in detail on the preparation and micromagnetic characterization of (Ga,Mn)As epilayers prepared in the Molecular Beam Epitaxy (MBE) laboratory in Prague [25]. We also pointed out that the preparation of (Ga,Mn)As by this highly nonequilibrium synthesis in two distinct MBE laboratories in Prague and in Nottingham led to a growth of epilayers with micromagnetic parameters that showed the same doping trends [25]. Nevertheless, the preparation of epilayers with identical parameters (e.g., thickness, nominal Mn content, etc.) in two distinct MBE machines is still a nontrivial task. Therefore, in this study of the role of the phosphorus incorporation to (Ga,Mn)As, we opted for a direct comparison of materials prepared in one MBE machine. The investigated $Ga_{1-x}Mn_xAs$ and $Ga_{1-x}Mn_xAs_{1-y}P_y$ epilayers were prepared in Nottingham [20] with the same nominal amount of Mn ($x = 6\%$) and the same growth time on a GaAs substrate [with a 50-nm-thick GaAsP buffer layer in the case of (Ga,Mn)(As,P)]. They differ only in the incorporation of P ($y = 10\%$) in the latter epilayer. The inferred epilayer thicknesses are (24.5 ± 1.0) nm for both (Ga,Mn)As and (Ga,Mn)(As,P) [29]. The as-grown layers, which both had the EA in the epilayer plane, were thermally annealed (for 48 hours at 180 °C). This led to an increase in Curie temperature and to a rotation of the EA to the perpendicular-to-plane orientation for (Ga,Mn)(As,P) [20,21].

The magnetic anisotropy of the samples was studied using a superconducting quantum interference device (SQUID) magnetometer and by the all-optical FMR [25]. The hole concentration was determined by fitting to Hall effect measurements at low temperatures (1.8 K) for external magnetic fields from 2 T to 6 T. In this range the magnetization is saturated, and one can obtain the normal Hall coefficient after correction for the field dependence of the anomalous Hall coefficient due to the weak magnetoresistance [30]. The time-resolved pump-and-probe MO experiments were performed using a titanium sapphire pulsed laser (pulse width ≈200 fs) with a repetition rate of 82 MHz, which was tuned ($h\upsilon = 1.64$ eV) above the GaAs band gap. The energy fluence of the pump pulses was around 30 μJcm^{-2}, and the probe pulses were at least 10 times weaker. The pump pulses were circularly polarized (with a helicity controlled by a quarter wave plate), and the probe pulses were linearly polarized (in a direction perpendicular to the external magnetic field). The time-resolved MO data reported here correspond to the polarization-independent part of the pump-induced rotation of probe polarization plane, which was computed from the measured data by averaging the signals obtained for the opposite helicities of circularly polarized pump pulses [27,28]. The experiment was performed close to the normal-incidence geometry, where the angles of incidence were 9° and 3° (measured from the sample normal) for the probe and the pump pulses, respectively.

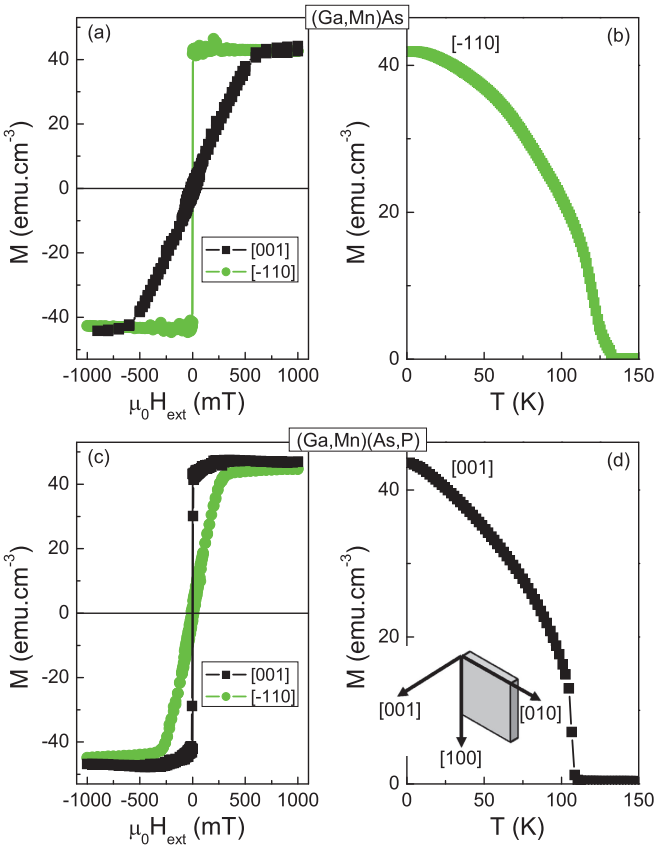

FIG. 1. (Color online) Magnetic characterization of samples: (a), (b) (Ga,Mn)As and (c), (d) (Ga,Mn)(As,P). (a), (c) Hysteresis loops measured in at 2 K for the external magnetic field applied in the sample plane (along the crystallographic direction [−110]) and perpendicular to sample plane (along the crystallographic direction [001]). (b), (d) Temperature dependence of the remanent magnetization. Inset: Definition of the coordinate system.

The rotation of the probe polarization plane is caused by two MO effects—the polar Kerr effect and the magnetic linear dichroism, which are sensitive to perpendicular-to-plane and in-plane components of magnetization, respectively [31–33]. For all MO experiments, samples were mounted in a cryostat and cooled down to ≈15 K. The cryostat was placed between the poles of an electromagnet, and the external magnetic field H_{ext} ranging from ≈0 to 585 mT was applied in the sample plane, either in the [010] or [110] crystallographic direction of the sample (see inset in Fig. 1 for a definition of the coordinate system). Prior to all measurements, we always prepared the magnetization in a well-defined state by first applying a strong saturating magnetic field and then reducing it to the desired magnitude of H_{ext}.

III. RESULTS AND DISCUSSION

A. Sample characterization

The hysteresis loops measured by SQUID magnetometry for the external magnetic field applied along the in-plane

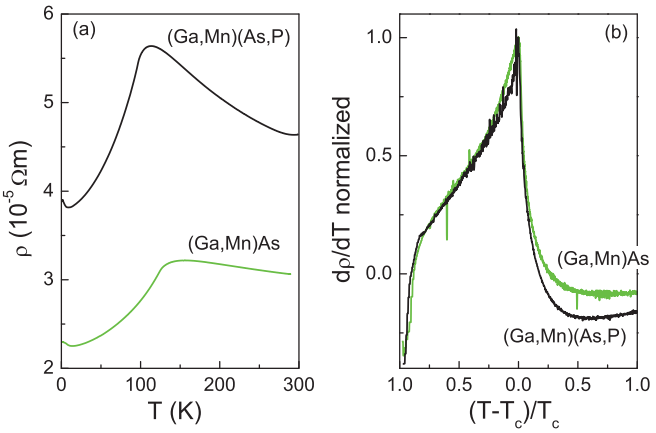

FIG. 2. (Color online) Electrical characterization of samples. Temperature dependence of the resistivity (a) and its temperature derivative (b).

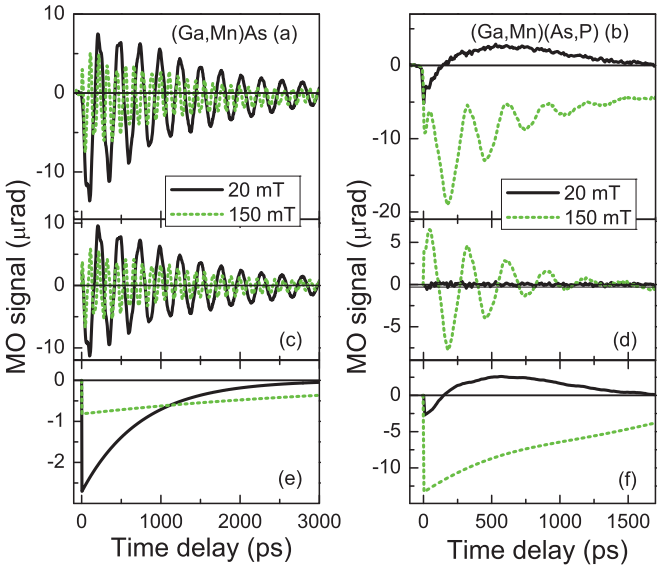

FIG. 3. (Color online) Time-resolved MO signals measured in (Ga,Mn)As (a) and (Ga,Mn)(As,P) (b) for two magnitudes of the external magnetic field applied along the [010] crystallographic direction. The measured MO signals were decomposed into oscillatory parts [(c), (d)], which correspond to the magnetization precession, and to nonoscillatory parts [(e), (f)], which are connected with the quasiequilibrium tilt of the EA and with the demagnetization. Note different x scales in the left and in the right columns.

[−110] and perpendicular-to-plane [001] crystallographic directions in (Ga,Mn)As and (Ga,Mn)(As,P) samples are shown in Figs. 1(a) and 1(c), respectively. These data confirm the expected in-plane and perpendicular-to-plane orientations of the EA in (Ga,Mn)As and (Ga,Mn)(As,P), respectively. Moreover, they reveal that for the (Ga,Mn)(As,P) sample, an external magnetic field of ≈250 mT is needed to rotate the magnetization into the sample plane. In Figs. 1(b) and 1(d), we show the temperature dependences of the remanent magnetization of the samples from which the Curie temperature T_c of ≈130 K and ≈110 K can be deduced. The measured saturation magnetization also indicates very similar density of Mn moments contributing to the FM state in the two samples.

The electrical characterization of the samples is shown in Fig. 2. The measured data show a sharp Curie point singularity in the temperature derivative of the resistivity. The presence of the Curie point singularities in magnetization [Fig. 1(d)] and electrical transport [Fig. 2(b)] measurements is a clear signature of the uniform, high-quality itinerant ferromagnet that is an essential requirement for a reliable determination of intrinsic properties of (Ga,Mn)(As,P) [25]. As we have shown recently, seemingly small departures from the optimized growth protocols can conceal the intrinsic properties of (Ga,Mn)As (see Fig. 1 in Ref. [25]). In the previously published papers about (Ga,Mn)(As,P), the detailed characterization of the samples (similar to that shown in Figs. 1 and 2) is usually not provided. Despite this fact, the lower magnetic quality of the previously studied samples is immediately apparent from their lower T_c: For example, in samples used in Ref. [13], the Curie temperature in the sample with higher Mn (7%) and lower P (7%) contents—with respect to that in our sample—was only 80 K. (Recall that both the Mn concentration increase and the P concentration decrease should *increase* [13] the Curie temperature, which in our sample is 110 K). In Ref. [19], T_c as low as 60 K was reported.

The hole densities inferred from Hall measurements are $(1.3 \pm 0.2)\times 10^{21}$ cm^{-3} and $(0.8 \pm 0.2)\times 10^{21}$ cm^{-3} for (Ga,Mn)As and (Ga,Mn)(As,P), respectively. The hole density obtained for (Ga,Mn)As is in agreement with our previous measurements for similar films in magnetic fields up 14 T [30]. The reduction of the density of itinerant holes quantitatively correlates with the observed increase of the resistivity of the (Ga,Mn)(As,P) film as compared to the (Ga,Mn)As sample.

B. Time-resolved MO experiment

In Figs. 3(a) and 3(b), we show the measured MO signals that reflect the magnetization dynamics in (Ga,Mn)As and (Ga,Mn)(As,P) samples, respectively. These signals can be decomposed into the oscillatory parts [Figs. 3(c) and 3(d)] and the nonoscillatory pulselike background [Figs. 3(e) and 3(f)] [27,28]. The oscillatory part arises from the precessional motion of magnetization around the quasiequilibrium EA, and the pulselike function reflects the laser-induced tilt of the EA and the laser-induced demagnetization [25,31]. The pump polarization-independent MO data reported here, which were measured at a relatively low excitation intensity of 30 μJcm^{-2}, can be attributed to the magnetization precession induced by a transient heating of the sample due to the absorption of the laser pulse [8,9]. Before absorption of the pump pulse, the magnetization is along the EA direction. Absorption of the laser pulse leads to a photoinjection of electron-hole pairs. The subsequent fast nonradiative recombination of photoinjected electrons induces a transient increase of the lattice temperature (within tens of picoseconds after the impact of the pump pulse). The laser-induced change of the lattice temperature then leads to a change of the EA position [34]. As a result, magnetization starts to follow the EA shift by the precessional motion. Finally, dissipation of the heat leads to a return of the EA to the equilibrium position, and the precession of magnetization is stopped by a Gilbert damping [25]. It is apparent from Fig. 3 that the measured

MO signals are strongly dependent on a magnitude of the external magnetic field, which was applied in the epilayer plane along the [010] crystallographic direction in both samples. In particular, absorption of the laser pulse does not induce precession of magnetization in (Ga,Mn)(As,P) unless magnetic field stronger than 20 mT is applied [see Fig. 3(d)].

The magnetization dynamics is described by the Landau-Lifshitz-Gilbert (LLG) equation that is usually expressed in the form [35,36]:

$$\frac{d\boldsymbol{M}(t)}{dt} = -\gamma[\boldsymbol{M}(t) \times \boldsymbol{H}_{\text{eff}}(t)] + \frac{\alpha}{M_s}\left[\boldsymbol{M}(t) \times \frac{d\boldsymbol{M}(t)}{dt}\right], \tag{1}$$

where $\gamma = (g\mu_B)/\hbar$ is the gyromagnetic ratio, g is the g factor, μ_B is the Bohr magneton, $\hbar$ is the reduced Planck constant, α is the Gilbert damping constant, and H_{eff} is the effective magnetic field. Nevertheless, it is more convenient to express this equation in spherical coordinates where the direction of the magnetization vector $\boldsymbol{M}$ is given by the polar angle θ and azimuthal angle φ and where H_{eff} can be directly connected with angular derivatives of the functional of magnetic energy density F (see the Appendix) [37]. For small deviations $\delta\theta$ and $\delta\varphi$ of magnetization from its equilibrium position (given by θ_0 and φ_0), the solution of the LLG equation can be written in the form $\theta(t) = \theta_0 + \delta\theta(t)$ and $\varphi(t) = \varphi_0 + \delta\varphi(t)$ as

$$\theta(t) = \theta_0 + A_\theta e^{-k_d t}\cos(2\pi f t + \Phi), \tag{2}$$

$$\varphi(t) = \varphi_0 + A_\varphi e^{-k_d t}\sin(2\pi f t + \Phi), \tag{3}$$

where the constants A_θ (A_φ) represent the amplitude of $\theta(\varphi)$, respectively, Φ is the initial phase, f is the magnetization precession frequency, and k_d is the precession damping rate (see the Appendix). The precession frequency reflects the internal magnetic anisotropy of the sample that can be characterized by the cubic (H_C), in-plane uniaxial (H_u), and out-of-plane uniaxial (H_{out}) anisotropy fields [see Eq. (A4) in the Appendix] [10]. Moreover, f depends also on the magnitude and on the orientation of H_{ext} (see the Appendix); therefore, the magnetic field dependence of f can be used to evaluate the magnetic anisotropy fields in the sample. If the applied in-plane magnetic field is strong enough to align the magnetization parallel with H_{ext} (i.e., for H_{ext} exceeding the saturation field in the sample for a particular orientation of H_{ext}), $\theta = \theta_H = \pi/2$ and $\varphi = \varphi_H$, and if the precession damping is relatively slow, i.e., $\alpha^2 \approx 0$, f can be expressed as

$$f = \frac{g\mu_B\mu_0}{h}\sqrt{\left(H_{\text{ext}} - 2H_{\text{out}} + \frac{H_C(3+\cos 4\varphi)}{2} + 2H_u\sin^2\left(\varphi_H - \frac{\pi}{4}\right)\right)(H_{\text{ext}} + 2H_C\cos 4\varphi_H - 2H_u\sin 2\varphi_H)}. \tag{4}$$

In Fig. 4 we show the fast Fourier transform (FFT) spectra of the oscillatory parts of the MO signals measured in the (Ga,Mn)As sample for different values of H_{ext}. This figure clearly reveals that for all external magnetic fields there are two distinct oscillatory frequencies present in the measured data. These precession modes are the SWRs, i.e., spin waves (or magnons) that are selectively amplified by fulfilling the boundary conditions. In general, different magnetic boundary conditions lead to a different character of SWRs [26,38–45]. In our case of a magnetically homogeneous [25] thin magnetic film with a thickness L, SWRs correspond to so-called perpendicular standing spin waves (PSSWs) where the wave vector k is quantized as $k = n\pi/L$ (where n is the mode number) [38–41]. The applied all-optical pump-probe technique gives no k selectivity, as discussed in Refs. [38,39], and references therein. In the theoretical treatment of spin waves, PSSWs are obtained when the magnetic boundary conditions corresponding to a "free surface" with $\delta M_{x,y}/\delta z = 0$ are considered [42]. In this case, the mode with $n = 0$ (at frequency f_0) corresponds to the uniform magnetization precession with zero k vector (i.e., the precession where at any instant of time all magnetic moments are parallel over the entire sample). The schematic depiction of modes with $n = 0$ (at frequency f_0) and $n = 1$ (at frequency f_1) will be shown in the inset of Fig. 8 (modes with higher n are shown, for example, in Fig. 1 in Ref. [39] and in Fig. 5 in Ref. [42]). The assessment of the experimentally observed SWRs to PSSWs is based on our experiments in optimized GaMnAs epilayers, which are very similar to those used in this paper, which we have reported recently in Ref. [25]. In particular, we prepared three samples by etching the original 48-nm-thick (Ga,Mn)As film down to thicknesses of 39, 29, and 15 nm, and we studied them by the optical FMR [25]. First, we observed that the frequency of the lowest mode f_0 was independent of the film thickness [see Fig. 6(b) in Ref. [25]], which confirms that it corresponds to the uniform precession mode. Moreover, the observed independence of f_0 on the film thickness confirms the magnetic homogeneity of our sample along the growth

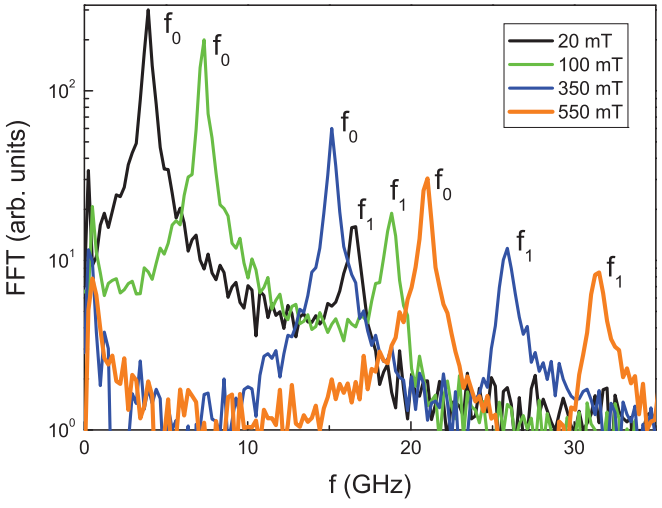

FIG. 4. (Color online) Fourier spectrum of the oscillatory part of the MO signal measured in (Ga,Mn)As for external magnetic fields applied along the [010] crystallographic direction. f_0 and f_1 indicate the frequencies of the uniform magnetization precession and the first SWR, respectively.

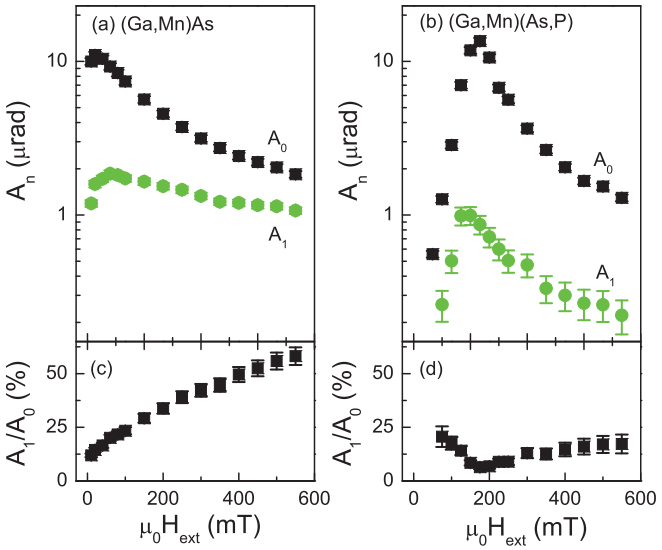

FIG. 5. (Color online) Dependence of the amplitude of the uniform magnetization precession (A_0) and the first SWR (A_1) on the magnitude of the external magnetic field (H_{ext}) applied along the [010] crystallographic direction in (Ga,Mn)As (a) and (Ga,Mn)(As,P) (b). (c), (d) Dependence of the ratio A_1/A_0 on H_{ext}.

direction (cf. Fig. 1 in Ref. [26] where a considerable change of the magnetic anisotropy along the growth direction was clearly apparent). Second, we observed the expected quadratic spacing of the SWR modes both in the mode number and in the sample thickness [see Figs. 6(d) and 6(e) in Ref. [25] and also the discussion in Sec. III D below]. Finally, we note that the *simultaneous* observation of modes with $n = 0$, 1, and 2 (see Fig. 6 in Ref. [25]) is an experimental proof that the all-optical pump-probe technique gives no k selectivity not only in metals [38,39], where the penetration depth of light is smaller than the metal layer thickness, but also in semiconductors, where penetration depth of light is much larger than the layer thickness.

In the present case of the FM films of (Ga,Mn)As and (Ga,Mn)(As,P) with a thickness around 25 nm, we detect only two modes. In Fig. 5, we plot the amplitudes of the uniform magnetization precession (A_0) and of the first SWR (A_1) as a function of the external magnetic field H_{ext}. In the (Ga,Mn)As sample, the oscillations are present even when no magnetic field is applied, and the precession amplitude increases slightly with an increasing H_{ext} (up to ≈20 mT for A_0 and up to ≈60 mT for A_1). Above this value, a further increase of H_{ext} leads to a suppression of the oscillations, but the suppression of the first SWR is slower than that of the uniform magnetization precession [see Fig. 5(c)]. In (Ga,Mn)(As,P), the oscillatory signal starts to appear at ≈50 mT, reaches its maximum for $\mu_0 H_{ext} \approx 175$ mT, and a further increase of H_{ext} leads to its monotonic decrease, like in the case of (Ga,Mn)As. The observed field dependence of the precession amplitude, which expresses the sensitivity of the EA position on the laser-induced sample temperature change, can be qualitatively understood as follows. In (Ga,Mn)As, the position of the EA in the sample plane is given by a competition between the cubic and the in-plane uniaxial magnetic anisotropies [10,25]. The laser-induced heating of the sample leads to a reduction of the magnetization magnitude M, and, consequently, it enhances the uniaxial anisotropy relative to the cubic anisotropy [9]. This is because the uniaxial anisotropy component scales with magnetization as $\sim M^2$, while the cubic component scales as $\sim M^4$. The application of H_{ext} along the [010] crystallographic direction deepens the minimum in the [010] direction in the functional of magnetic energy density F [due to the Zeeman term in F, see Eq. (A4) in the Appendix]. Measured data shown in Fig. 5 reveal that in the (Ga,Mn)As sample, H_{ext} initially (for fields up to ≈20 mT) destabilizes the position of EA but stabilizes it for large values of H_{ext} (where the position of the energy minimum in F is dominated by the Zeeman term, which is not temperature dependent). In the case of (Ga,Mn)(As,P), the position of the EA is determined by the strong perpendicular-to-plane anisotropy. Therefore, without an external magnetic field, the laser-induced heating of the sample does not change significantly the position of EA and, consequently, does not initiate the precession of magnetization [see Fig. 5(b)]. The application of an in-plane field moves the energy minimum in F towards the sample plane [see Fig. 1(c)], which makes the EA position more sensitive to the laser-induced temperature change. Finally, for a sufficiently strong H_{ext}, the sample magnetic anisotropy is dominated by the temperature-independent Zeeman term, which again suppresses the precession amplitude. The markedly different ratio A_1/A_0 in the (Ga,Mn)As and (Ga,Mn)(As,P) samples remains unclear at present. However, it can be connected with a slight surface anisotropy effect and/or a difference in magnetic homogeneity in these two samples [43,44].

C. Determination of magnetic anisotropy

In Fig. 6 we plot the magnetic field dependences of f_0 and f_1 for two different orientations of H_{ext}. The frequency f_0 of the spatially uniform precession of magnetization is given by Eq. (4). For the SWRs, where the local moments are no longer parallel (as will be seen in the inset in Fig. 8), restoring torques

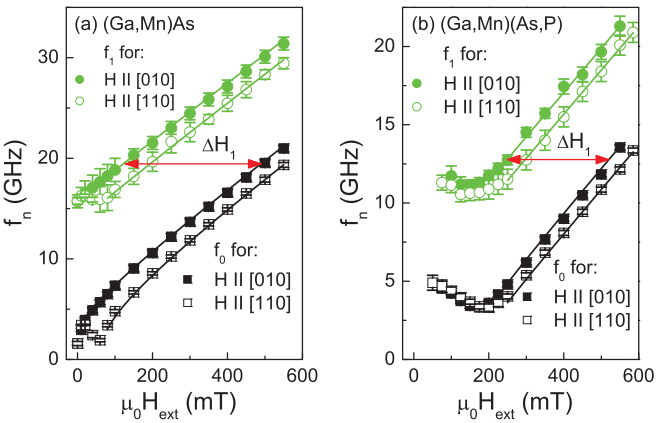

FIG. 6. (Color online) Magnetic field dependence of the precession frequencies f_0 and f_1 for two different orientations of the external magnetic field (points) measured in (Ga,Mn)As (a) and (Ga,Mn)(As,P) (b). Lines are the fits by Eqs. (5) and (6). ΔH_1 indicates the shift of the resonant field for the first spin-wave mode with respect to the uniform precession mode.

due to exchange interaction and internal magnetic dipolar interaction have to be included in the analysis [39–41,45]. For H_{ext} along the [010] crystallographic direction (i.e., for $\varphi_H = \pi/2$), Eq. (4) can be written as

$$f_n = \frac{g\mu_B\mu_0}{h}\sqrt{(H_{\text{ext}} - 2H_{\text{out}} + H_c + \Delta H_n)(H_{\text{ext}} - 2H_c - 2H_u + \Delta H_n)}, \tag{5}$$

where ΔH_n is the shift of the resonant field for the nth spin-wave mode with respect to the $n = 0$ uniform precession mode. Analogically, for H_{ext} applied in the [110] crystallographic direction (i.e., for $\varphi_H = \pi/4$)

$$f_n = \frac{g\mu_B\mu_0}{h}\sqrt{(H_{\text{ext}} - 2H_{\text{out}} + 2H_c + H_u + \Delta H_n)(H_{\text{ext}} + 2H_c + \Delta H_n)}. \tag{6}$$

The lines in Fig. 6 represent the fits of all four measured dependencies $f_n = f_n\,(H_{\text{ext}}, \varphi_H)$ [where $n = 0$; 1 and $\varphi_H = \pi/4$; $\pi/2$] with a single set of anisotropy constants for each of the samples, which confirms the credibility of the fitting procedure. The obtained anisotropy fields at ≈15 K are $\mu_0 H_C = (17 \pm 3)$ mT, $\mu_0 H_u = (11 \pm 5)$ mT, $\mu_0 H_{\text{out}} = (-200 \pm 20)$ mT for (Ga,Mn)As and $\mu_0 H_C = (14 \pm 3)$ mT, $\mu_0 H_u = (11 \pm 5)$ mT, $\mu_0 H_{\text{out}} = (90 \pm 10)$ mT for (Ga,Mn)(As,P), respectively (in both cases we considered the Mn g factor of 2). Note that the experimentally measured total effective out-of-plane anisotropy field H_{out} is actually a sum of the out-of-plane magneto-crystalline anisotropy field of the sample and of the contribution of the demagnetization field ($H_{\text{demag}} = -4\pi M$) of the FM film [40]. The latter contribution corresponds to ≈−50 mT both for (Ga,Mn)As and (Ga,Mn)(As,P) samples. For (Ga,Mn)As, we can now compare the determined anisotropy constants with those obtained by the same fitting procedure for samples prepared in a different MBE laboratory (in Prague)—see Fig. 4 in Ref. [25]. We see that the previously reported [25] doping trends of H_C and H_{out} predict for a sample with nominal Mn doping $x = 6\%$ the anisotropy fields, which are the same as those reported in this paper for the sample grown in Nottingham. This observation is in accord with the current microscopic understanding of their origin: H_C reflects the zinc-blende crystal structure of the host semiconductor and H_{out} is a sum of the anisotropy due to the growth-induced lattice-matching strain and of the thin-film shape anisotropy, which should be the same for equally doped and optimally synthesized samples, independent of the growth chamber. On the other hand, the microscopic origin of in-plane uniaxial anisotropy field H_u is still not established [10,25], and our data reveal that it is considerably smaller in the sample grown in Nottingham. We observed that the incorporation of phosphorus does not change significantly the values of H_C and H_u, but it strongly modifies the magnitude and changes the sign of H_{out}. This observation is in qualitative agreement with the previously reported FMR study where 50-nm-thick samples of $Ga_{1-x}Mn_xAs_{1-y}P_y$ with $x \approx 0.07$ and y from 0 to ≈0.09 (and the Curie temperature between 110 and 135 K) were studied [22]. For example, incorporation of ≈9% P led at 4 K to a change of $\mu_0 H_{2\perp}$ from ≈− 350 mT to ≈ +300 mT, while other anisotropy fields were not modified significantly [22].

D. Determination of spin stiffness

The spin stiffness is associated with the exchange energy of non-uniform local directions of the magnetization, in particular with the energy of small wave-vector spin-wave excitations of the ferromagnet. Considering a specific model of thermodynamic properties of the studied ferromagnet, the spin stiffness can be indirectly inferred from the measured temperature dependence of magnetization [46], Curie temperature [46], or DW width [47]. The direct determination of the spin stiffness from magnetization dynamics experiments is significantly more challenging than in the case of the magnetic anisotropy fields. The low-energy nonuniform collective excitations of the system can be strongly affected by inhomogeneities or surface properties of the ferromagnet for which specific models have to be assumed in order to extract the spin stiffness constant from the measured data. Exceptions are the PSSW modes of a uniform thin-film ferromagnet for which the spin stiffness parameter D is directly obtained from the measured resonant fields (see below). There are many reports of SWR measurements in (Ga,Mn)As on >100-nm-thick epilayers using FMR [26,43,48,49]. The modes with $\Delta H_n \sim n^2$ were observed only in a 120-nm-thick, 8% Mn-doped (Ga,Mn)As for magnetic fields applied close to the magnetic EA [43]. Measurements of the same sample in other field orientations showed different trends, which indicated the presence of strong inhomogeneities and surface dependent effects [43]. A linear or sublinear dependence of the resonant fields on the mode index has been reported also in the other FMR measurements of thick (Ga,Mn)As epilayers [25,26,43,48,49]. The extracted values of the spin stiffness constant D from all available magnetic resonance [26,43,44,49] data in (Ga,Mn)As materials, complemented by values inferred from magnetization and domain studies [46,47], are scattered over more than an order of magnitude and show no clear trend as a function of Mn doping or other material parameters of the (Ga,Mn)As FM semiconductor (see Fig. 12 in Ref. [50]).

In our case of optimised GaMnAs epilayers, the observation of a higher order PSSW enables us to determine the exchange spin stiffness constant D from the field mode spacing ΔH_n [25]. In magnetically homogeneous thin films with negligible surface anisotropy, ΔH_n is given by [39]

$$\Delta H_n \equiv H_0 - H_n = n^2 \frac{D}{g\mu_B\mu_0}\frac{\pi^2}{L^2}, \tag{7}$$

where L is the thickness of the magnetic film. Note that we have confirmed experimentally the validity of Eq. (7) for the field mode spacings measured in optimized GaMnAs epilayers [25]. In particular, we have observed the expected quadratic spacing of the SWR modes both in the mode number and in the sample thickness [see Figs. 6(d) and 6(e), respectively, in Ref. [25]]. Moreover, we have verified that the same value of D can be deduced from the n dependence of the resonant field spacings

in the $L = 48$ nm epilayer and from the L dependence of ΔH_1 [25].

By fitting the data in Fig. 6, we obtained $\mu_0 \Delta H_1 = (363 \pm 2)$ mT for (Ga,Mn)As and (271 ± 2) mT for (Ga,Mn)(As,P), which correspond to $D = (2.5 \pm 0.2)$ meVnm^2 and (1.9 ± 0.2) meVnm^2 for (Ga,Mn)As and (Ga,Mn)(As,P), respectively (note that the relatively large experimental error in D is given mainly by the uncertainty of the epilayer thickness) [29]. The value of D obtained for (Ga,Mn)As is in agreement with that reported previously for samples grown in Prague [25], which also confirms the consistent determination of the epilayer thicknesses in both MBE laboratories [29]. Our results reveal that the incorporation of phosphorus leads to a reduction of D, which correlates with the decrease of the hole density [51], and the reduced T_c in (Ga,Mn)(As,P), as compared to its (Ga,Mn)As counterpart. Up to now, there are only two reports about the spin stiffness measurements in (Ga,Mn)(As,P) [13,22]. In Ref. [22], the value $D = 0.317$ meVnm^2 was evaluated from the FMR study at 40 K using the sample with 7% Mn (the amount of P in the sample used for the D determination is not clearly specified in Ref. [22]). On the other hand, in Ref. [13] the exchange konstant $A \approx 0.42$ pJ.m^{-1} was evaluated from the period of self-organized magnetic domains in sample with 10% Mn and 7% P at 4 K. This corresponds, considering [13] a 10% contribution of holes opposite to magnetization, to $D \approx 1.6$ meVnm^2 which is in a reasonably good agreement with the value that we determined in the (Ga,Mn)(As,P) sample. The same group applied the identical experimental technique also for a sample with 7% of Mn without P, and they obtained [13,47] $D \approx 0.5$ meVnm^2. These measurements [13,47] might seem to indicate that incorporation of P increases significantly the spin stiffness, which is a clear contrast with our observation that incorporation of P decreases the spin stiffness slightly. The most plausible explanation of this discrepancy is the lower magnetic quality of the (Ga,Mn)As sample used in Ref. [47]: in their sample, with 7% of Mn they observed $T_c = 130$ K and $M_S \approx 38$ emu.cm^{-3}, while in our optimized films we have [25] for 7% of Mn $T_c = 159$ K and $M_S = 57$ emu.cm^{-3}.

E. Determination of Gilbert damping

The Gilbert damping constant α can be determined by fitting the measured dynamical MO signals by the LLG equation [35,36,52]. For a relatively slow precession damping and a sufficiently strong external magnetic field, the analytical solution of the LLG equation gives (see the Appendix)

$$k_d = \alpha \frac{g\mu_B\mu_0}{2\hbar}\left(2H_{\text{ext}} - 2H_{\text{out}} + \frac{H_C(3+5\cos 4\varphi_H)}{2} + H_u(1-3\sin 2\varphi_H)\right). \quad (8)$$

Equation (8) shows not only that k_d is proportional to α but also that for obtaining a correct value of α from the measured MO precession signal damping it is necessary to take into account a realistic magnetic anisotropy of the investigated sample. Nevertheless, the correct dependence of k_d on magnetic anisotropy was not considered in the previous studies [35,36,52], where only one effective magnetic field was used, which is probably one of the reasons why mutually inconsistent results were obtained for $Ga_{1-x}Mn_xAs$ with a different Mn content x. An increase of α from $\approx$0.02 to $\approx$0.08 for an increase of x from 3.6% to 7.5% was reported in Ref. [36]. On the contrary, in Ref. [52] values of α from 0.06 to 0.19—without any apparent doping trend—were observed for x from 2% to 11%. Another plausible explanation of this discrepancy might be the role of the extrinsic damping on the measured magnetization precession: the precession signal can be quenched not only due to the intrinsic Gilbert damping but also due to the extrinsic mechanisms [53–55]. To address this issue, in the following we call the damping constant, which was deduced by modeling from the experimentally measured MO dynamics, "apparent damping constant" α', and we reserve the term "Gilbert damping constant" α for its frequency-independent part [56,57].

For numerical modeling of the measured MO data, we first computed from the LLG equation [Eqs. (A1) and (A2) in the Appendix with the measured magnetic anisotropy fields] the time-dependent deviations of the spherical angles [$\delta\theta(t)$ and $\delta\varphi(t)$] from the corresponding equilibrium values (θ_0, φ_0). Then we calculated how such changes of θ and φ modify the static MO response of the sample, which is the signal that we detect experimentally [31]

$$\begin{aligned}\delta\text{MO}(\Delta t,\beta) &= -\delta\theta(\Delta t)\,P^{\text{PKE}} + \delta\varphi(\Delta t)\,P^{\text{MLD}} 2\cos 2(\varphi_0-\beta) \\ &\quad + \frac{\delta M_s(\Delta t)}{M_0}\,P^{\text{MLD}} 2\sin 2(\varphi_0-\beta). \end{aligned} \quad (9)$$

The first two terms in Eq. (9) are connected with the out-of-plane and in-plane movement of magnetization, and the last term describes a change of the static MO response of the sample due to the laser-induced demagnetization [31]. P^{PKE} and P^{MLD} are MO coefficients that describe the MO response of the sample, which we measured independently in a static MO experiment [32,33], and β is the probe polarization orientation with respect to the crystallographic direction [100] [31]. To further simplify the fitting procedure, we can extract the oscillatory parts from the measured MO data (cf. Fig. 3), which effectively removes the MO signals due to the laser-induced demagnetization [i.e., the last term in Eq. (9)] and due to the in-plane movement of the EA [i.e., a part of the MO signal described by the second term in Eq. (9)] [31]. Examples of the fitting of the precessional MO data are shown in Figs. 7(a) and 7(b) for (Ga,Mn)As and (Ga,Mn)(As,P), respectively. We stress that in our case the only fitting parameters in the modeling are the damping coefficient α' and the initial deviations of the spherical angles from the corresponding equilibrium values. By this numerical modeling, we deduced a dependence of the apparent damping constant α' on the external magnetic field for two different orientations of H_{ext}. At smaller fields, the dependences obtained show a strong anisotropy with respect to the field angle that can be fully ascribed to the field-angle dependence of the precession frequency [25]. However, when plotted as a function of the precession frequency, the dependence on the field-angle disappears [see Figs. 7(c) and 7(d) for (Ga,Mn)As and (Ga,Mn)(As,P), respectively]. For both materials, α' initially decreases monotonously with f, and finally

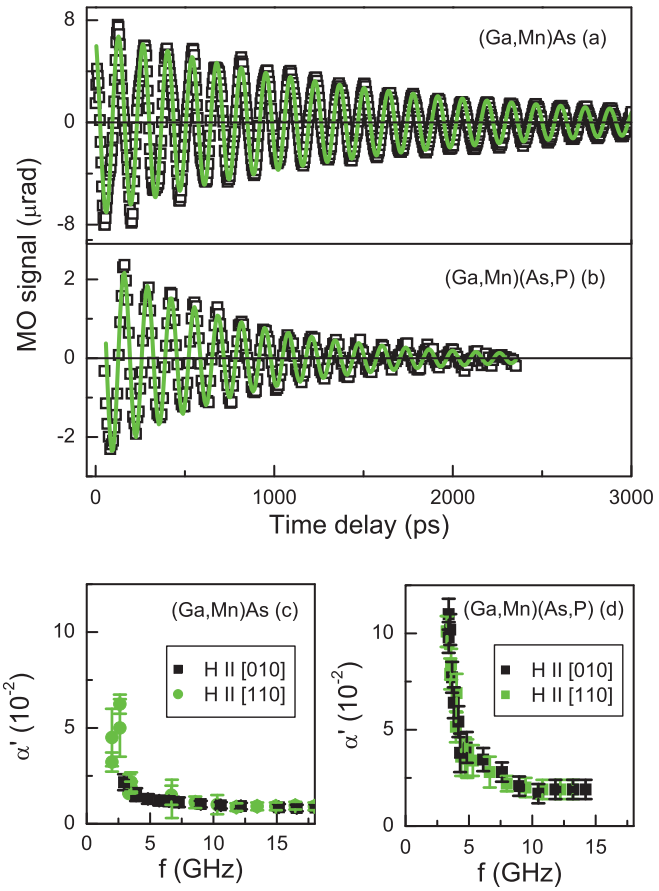

FIG. 7. (Color online) Determination of the Gilbert damping. (a), (b) Oscillatory part of the MO signal (points) measured in (Ga,Mn)As for the external magnetic field 100 mT (a) and in (Ga,Mn)(As,P) for 350 mT (b); magnetic field applied along the [010] crystallographic direction leads to a similar frequency ($f_0 \approx 7.5$ GHz) in both cases. Lines are fits by the LLG equation. (c), (d) Dependence of the apparent damping constant (α') on the precession frequency for two different orientations of the external magnetic field in (Ga,Mn)As (c) and (Ga,Mn)(As,P) (d); the intrinsic Gilbert damping constant (α) is the frequency-independent part of α'.

it saturates at a certain value for $f \geqslant 10$ GHz. A frequency-dependent (or magnetic field-dependent) damping parameter was reported in various magnetic materials, and a variety of underlying mechanisms responsible for it were suggested as an explanation [53–55]. In our case, the most probable explanation seems to be the one that was used by Walowski *et al.* [53] to explain the experimental results obtained in thin films of nickel. They argued that in the low field range, small magnetization inhomogeneities can be formed—the magnetization does not align parallel in an externally applied field, but forms ripples [53]. Consequently, the measured MO signal that detects sample properties averaged over the laser spot size, which is in our case about 30 μm wide [full width at half-maximum (FWHM)], experiences an extrinsic oscillation damping because the magnetic properties (i.e., the precession frequencies) are slightly differing within the spot size (see Figs. 6 and 7 in Ref. [53]). On the other hand, for stronger external fields the sample is fully homogeneous; therefore, the precession damping is not dependent on the applied field (the precession frequency), as expected for the intrinsic Gilbert damping constant α [56,57]. We note that the observed monotonous frequency decrease of α' is in fact a signature of a magnetic homogeneity of the studied epilayers [25]. The obtained intrinsic Gilbert damping constants α (i.e., the frequency-independent values of α') are $(0.9 \pm 0.2)\times 10^{-2}$ for (Ga,Mn)As and $(1.9 \pm 0.5)\times 10^{-2}$ for (Ga,Mn)(As,P), respectively. The observed enhancement of the magnetization precession damping due to the incorporation of phosphorus is also clearly apparent directly from Figs. 7(a) and 7(b), where the MO data with similar precession frequencies are shown for (Ga,Mn)As and (Ga,Mn)(As,P), respectively. In (Ga,Mn)As, the value of α obtained is again fully in accord with the reported Mn doping trend in α in this material [25]. Up to now, there is only one report about the precession damping evaluation in (Ga,Mn)(As,P): in Ref. [22], the value $\alpha \approx 0.012$ was obtained from a FMR experiment sample with 7% Mn and 8.8% P, which is rather similar to the value that we determined for the (Ga,Mn)(As,P) sample. The observed increase of the intrinsic Gilbert damping constant in (Ga,Mn)(As,P) compared to that in (Ga,Mn)As is in fact fully consistent with the previously reported doping trends in the series of optimized (Ga,Mn)As materials [25]. Even though both studied materials possess the same nominal amount of Mn ($x = 6\%$), they have a different hole density—the experimentally measured hole density in (Ga,Mn)(As,P) is only ≈60% of that in (Ga,Mn)As. Such a value of the hole density would be present in (Ga,Mn)As material with $x \approx 4\%$ [see Fig. 3(d) in Ref. [25]], where $\alpha \approx 0.02$ [see Fig. 4(b) in Ref. [25]], which is very similar to the value observed in (Ga,Mn)(As,P).

The high quality of our MO data enables us to evaluate not only the damping of the uniform magnetization precession, which is addressed above, but also the damping of the first SWR. To illustrate this procedure, we show in Fig. 8(a) the MO data measured for $\mu_0 H_{\text{ext}} = 250$ mT applied along the [010] crystallographic direction in (Ga,Mn)As. The experimental data (points) obtained can be fitted by a sum of two exponentially damped cosine functions (line), which enables us to separate, directly in a time domain, the contributions of the individual precession modes to the measured MO signal. In this particular case, the uniform magnetization precession occurs at a frequency $f_0 = 12.2$ GHz, and this precession mode is damped with a rate constant $k_{d0} = 0.79$ ns^{-1}. Remarkably, the first SWR, which has a frequency $f_1 = 23.0$ GHz, has a considerably larger damping rate constant $k_{d1} = 1.7$ ns^{-1}, see Fig. 8(b) where the contribution of individual modes are directly compared and also Fig. 8(c) where Fourier spectra computed from the measured MO data for two different ranges of time delays are shown. To convert the obtained damping rate constant k_{dn} to the apparent damping constant α'_n for the nth mode, we can use the generalized analytical solution of the LLG equation. For a sufficiently strong H_{ext} along the [010] crystallographic direction (i.e., when $\varphi \approx \varphi_H = \pi/2$), Eq. (8) can be written as

$$k_{dn} = \alpha'_n \frac{g\mu_B\mu_0}{2\hbar}(2H_{\text{ext}} + 2\Delta H_n - 2H_{\text{out}} + 2H_C + H_u). \tag{10}$$

For the case of MO data measured at $\mu_0 H_{\text{ext}} = 250$ mT, the damping constants obtained for modes with $n = 0$ and

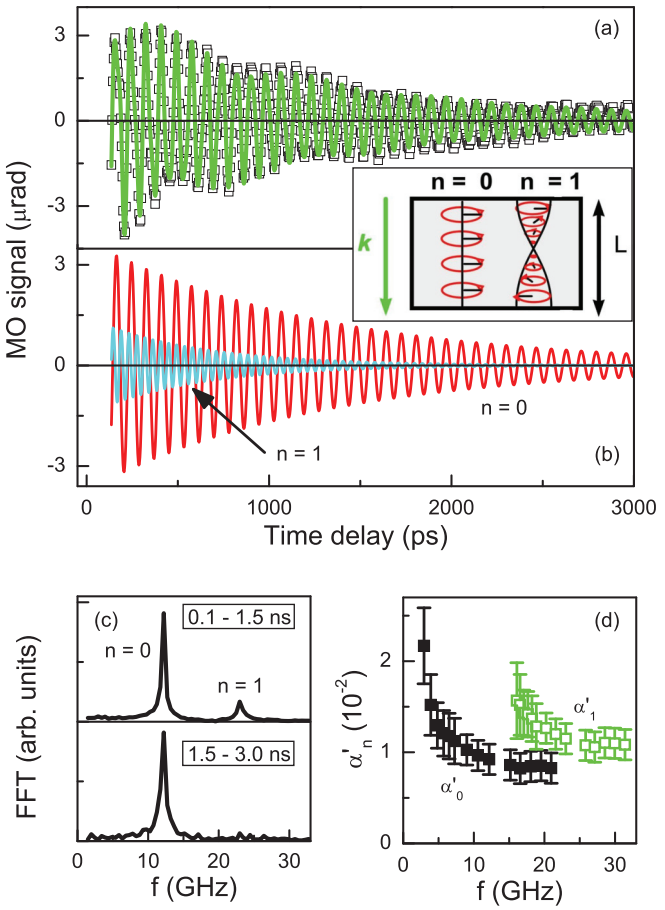

FIG. 8. (Color online) Comparison of the damping of the uniform magnetization precession and of the first SWR. (a) Oscillatory part of the MO signal (points) measured in (Ga,Mn)As for the external magnetic field 250 mT applied along the [010] crystallographic direction. The solid line is a fit by a sum of two exponentially damped cosine functions that are shown in (b). Inset: Schematic illustration (Refs. [39,42]) of the SWRs with $n = 0$ (uniform magnetization precession with zero k vector) and $n = 1$ (perpendicular standing spin wave with a wave vector k fulfilling the resonant condition $kL = \pi$) in a magnetic film with a thickness L. (c) Normalized Fourier spectra computed for the depicted ranges of time delays from the measured MO data, which are shown in (a). (d) Dependence of the apparent damping constant (α'_n) on the precession frequency for the uniform magnetization precession ($n = 0$) and the first SWR ($n = 1$).

1 are $\alpha'_0 = 0.009$ and $\alpha'_1 = 0.011$, respectively. [We note that the value of α_0 obtained from the analytical solution of LLG equation is identical to that determined by the numerical fitting that is shown in Fig. 7(c), which confirms the consistency of this procedure.] In Fig. 8(d), we show the dependence of α'_0 and α'_1 on the precession frequency. These data clearly show that for sufficiently high frequencies (i.e., external magnetic fields) the damping of the two modes is nearly equal [see Fig. 8(d)], as expected for intrinsic Gilbert damping. The different apparent damping of the modes at lower frequency can be again ascribed to the presence of an extrinsic contribution to the damping coefficient for the SWR modes. This extrinsic damping probably originates from small variations of the sample thickness (<1 nm) within the laser spot size [58] and/or from the presence of a weak bulk inhomogeneity [43], which is apparent as small variations of ΔH_n. The frequency spacing and the PSSW character of the SWR modes is insensitive to such small variations of ΔH_n, but the resulting frequency variations [see Eq. (5)] can still strongly affect the observed damping of the oscillations. For high enough external magnetic fields, the variations of ΔH_n have a negligible role and the damping of the SWR modes is for all modes governed solely by the intrinsic Gilbert damping parameter.

IV. CONCLUSIONS

We used the optical analog of FMR, which is based on a pump-and-probe MO technique, for the determination of micromagnetic parameters of (Ga,Mn)As and (Ga,Mn)(As,P) DMS materials. The main advantage of this technique is that it enables us to determine the anisotropy constants, the spin stiffness, and the Gilbert-damping parameter from a single set of the experimental MO data measured in films with a thickness of only several tens of nanometers. To address the role of phosphorus incorporation in (Ga,Mn)As, we measured simultaneously properties of (Ga,Mn)As and (Ga,Mn)(As,P) with 6% Mn doping, which were grown under identical conditions in the same MBE laboratory. We have shown that the laser-induced precession of magnetization is closely connected with a magnetic anisotropy of the samples. In particular, in (Ga,Mn)As with in-plane magnetic anisotropy the laser-pulse-induced precession of magnetization was observed even when no external magnetic field was applied. On the contrary, in (Ga,Mn)(As,P) with perpendicular-to-plane magnetic EA the precession of magnetization was observed only when the EA position was destabilized by an external in-plane magnetic field. From the measured MO data, we deduced the anisotropy constants, spin stiffness, and Gilbert-damping parameter in both materials. We have shown that the incorporation of 10% of P in (Ga,Mn)As leads not only to the expected sign change of the perpendicular-to-plane anisotropy field but also to a considerable increase of the Gilbert damping, which correlates with the increased resistivity and reduced itinerant hole density in the (Ga,Mn)(As,P) material. We also observed a reduction of the spin stiffness consistent with the suppression of T_c upon incorporating P in (Ga,Mn)As.

Alloying GaAs with substitutional Mn_{Ga} impurity on one hand and P_{As} on the other leads to distinct phenomenologies of the observed magnetic properties. This explains our distinct approaches to studying the effects of these two types of impurities. Mn_{Ga} is essential for turning the GaAs host semiconductor into a ferromagnet. The careful systematic study of the Mn_{Ga} doping trend is therefore of fundamental importance for elucidating the microscopic physics of the electronic and magnetic structure of the material and for addressing basic questions such as the highest achievable Curie temperature in this magnetic semiconductor. One of the original motivations for introducing P_{As} impurity was to explore whether the stronger magnetic coupling in a smaller lattice constant material can further enhance the Curie temperature [59]. No experiments have indicated, however, that alloying (Ga,Mn)As with P could indeed lead to the Curie temperature enhancement. On the other hand, several

groups discovered that the reduction of the lattice constant can reverse the sign of the strain in the magnetic semiconductor epilayer and by this can induce transition to a ferromagnet with an out-of-plane EA. This observation has facilitated fruitful research directions, including DW motion studies in a perpendicular magnetic material with exceptionally low extrinsic pinning. The key questions we aimed at addressing are therefore why P_{As} is not enhancing the Curie temperature and, if not improving the magnetic properties, whether the high magnetic, electrical, and structural quality of the parent (Ga,Mn)As ferromagnet can be at least preserved at a P_{As} doping density that is sufficient to safely turn the EA from the in-plane to the out-of-plane direction.

Reference [25] describes in detail the tedious optimization procedures for the synthesis of the highly nonequilibrium ternary alloys of (Ga,Mn)As and the essential role of the achieved sample quality for elucidating the intrinsic characteristics of this DMS. Optimizing the synthesis of a whole series of quaternary (Ga,Mn)(As,P) materials is an exceedingly complex task. For addressing the above two key materials questions and for demonstrating the applicability of our all-optical FMR technique for perpendicularly magnetized material, it is fully sufficient to choose a representative, optimally synthesized (Ga,Mn)(As,P) film with 10% P_{As} doping. From the all-optical FMR measurements on this sample, we can conclude that out-of-plane EA materials can be prepared by adding P, while other properties remain comparable to the optimized, high-quality parent (Ga,Mn)As material. We can also address the other key question that refers to the origin of the reduction of the Curie temperature upon adding P. The effect of the stronger magnetic coupling in the smaller lattice parameter (Ga,Mn)(As,P) is overcompensated by the observed decrease of the density of the itinerant holes and the associated decrease of the spin stiffness. These are the expected consequences of the increased binding energy of the Mn_{Ga} acceptor state in the larger band gap Ga(As,P) host.

ACKNOWLEDGMENTS

This work was supported by the Grant Agency of the Czech Republic Grant No. P204/12/0853, by the Grant Agency of Charles University in Prague Grants No. 1360313 and SVV-2013-267306, by the EU Grant European Research Council (ERC) Advanced Grant 268066-0MSPIN, by the European Metrology Research Programme (EMRP) within the Joint Research Project EXL04 SpinCal (the EMRP is jointly funded by the EMRP participating countries within EURAMET and the EU), by Praemium Academiae of the Agency of the Czech Republic, by the Ministry of Education of the Czech Republic Grant No. LM2011026, and by the Czech Science Foundation Grant No. 14-37427G.

APPENDIX

Due to symmetry reasons, it is convenient to rewrite the LLG equation given by Eq. (1) in spherical coordinates, where M_S describes the magnetization magnitude and polar θ and azimuthal φ angles characterize its orientation. We define the perpendicular-to-plane angle θ (in-plane angle φ) in such a way that it is counted from the [001] ([100]) crystallographic direction, and it is positive when magnetization is tilted towards the [100] ([010]) direction (see inset of Fig. 1 for the coordinate system definition). The time evolution of magnetization is given by [37]

$$\frac{dM_s}{dt} = 0, \tag{A1}$$

$$\frac{d\theta}{dt} = -\frac{\gamma}{(1+\alpha^2)M_s}\left(\alpha \cdot A + \frac{B}{\sin\theta}\right), \tag{A2}$$

$$\frac{d\varphi}{dt} = \frac{\gamma}{(1+\alpha^2)M_s\sin\theta}\left(A - \frac{\alpha \cdot B}{\sin\theta}\right), \tag{A3}$$

where $A = dF/d\theta$ and $B = dF/d\varphi$ are the derivatives of the functional of magnetic energy density F with respect to θ and φ, respectively. We express F in a form [10]

$$F = M_S\left[H_C\sin^2\theta\left(\tfrac{1}{4}\sin^2 2\varphi\sin^2\theta + \cos^2\theta\right) - H_{\text{out}}\cos^2\theta - \tfrac{H_u}{2}\sin^2\theta\,(1-\sin 2\varphi) - H_{\text{ext}}(\cos\theta\cos\theta_H + \sin\theta\sin\theta_H\cos(\varphi-\varphi_H))\right], \tag{A4}$$

where H_C, H_u, and H_{out} are the constants that characterize the cubic, uniaxial, and out-of-plane magnetic anisotropy fields in (Ga,Mn)As, respectively. In fact, H_{out} is a total effective out-of-plane anisotropy field that is a sum of the out-of-plane magneto-crystalline anisotropy field of the sample and of the contribution of the demagnetization field of the FM film ($H_{\text{demag}} = -4\pi M$) [40]. H_{ext} is the magnitude of the external magnetic field whose orientation is described by the angles θ_H and φ_H, which are again counted from the [001] and [100] crystallographic directions, respectively.

For small deviations $\delta\theta$ and $\delta\varphi$ from the equilibrium values θ_0 and φ_0, the solution of Eqs. (A2) and (A3) can be expressed [60,61] by Eqs. (2) and (3). For the geometry of our experiment, i.e., the in-plane orientation of the external magnetic field ($\theta_H = \pi/2$), the equilibrium orientation of magnetization is in the sample plane for (Ga,Mn)As ($\theta_0 = \pi/2$), and the same applies for (Ga,Mn)(As,P) if sufficiently strong external magnetic field (see Fig. 1) is applied ($\theta_0 \approx \theta_H = \pi/2$). In such conditions, the precession frequency f and the damping rate k_d are given [60,61] by the following equations

$$f = \frac{g\mu_B\mu_0}{h(1+\alpha^2)}\sqrt{\begin{aligned}&\left(H_{\text{ext}}\cos(\varphi-\varphi_H) - 2H_{\text{out}} + \tfrac{H_C(3+\cos 4\varphi)}{2} + 2H_u\sin^2\left(\varphi-\tfrac{\pi}{4}\right)\right)\\ &\times\left(H_{\text{ext}}\cos(\varphi-\varphi_H) + 2H_C\cos 4\varphi - 2H_u\sin 2\varphi\right)\\ &+\alpha^2\Big\{\left(H_{\text{ext}}\cos(\varphi-\varphi_H) - 2H_{\text{out}} + \tfrac{H_C(3+\cos 4\varphi)}{2} + 2H_u\sin^2\left(\varphi-\tfrac{\pi}{4}\right)\right)\\ &\times\left(H_{\text{ext}}\cos(\varphi-\varphi_H) + 2H_C\cos 4\varphi - 2H_u\sin 2\varphi\right)\\ &-\left(H_{\text{ext}}\cos(\varphi-\varphi_H) - H_{\text{out}} + \tfrac{H_C(3+5\cos 4\varphi)}{4} + \tfrac{H_u(1-3\sin 2\varphi)}{2}\right)^2\Big\}\end{aligned}} \tag{A5}$$

$$k_d = \alpha \frac{g\mu_B\mu_0}{2\hbar(1+\alpha^2)}\left(2H_{\text{ext}}\cos(\varphi-\varphi_H) - 2H_{\text{out}} + \frac{H_C(3+5\cos 4\varphi)}{2} + H_u(1-3\sin 2\varphi)\right) \quad \text{(A6)}$$

[1] T. Jungwirth, J. Sinova, J. Mašek, J. Kučera, and A. H. MacDonald, Rev. Mod. Phys. **78**, 809 (2006).

[2] H. Ohno, Nat. Mater. **9**, 952 (2010).

[3] T. Dietl, Nat. Mater. **9**, 965 (2010).

[4] T. Dietl and H. Ohno, Rev. Mod. Phys. **86**, 187 (2014).

[5] T. Jungwirth, J. Wunderlich, V. Novak, K. Olejnik, B. L. Gallagher, R. P. Campion, K. W. Edmonds, A. W. Rushforth, A. J. Ferguson, and P. Nemec, Rev. Mod. Phys. **86**, 855 (2014).

[6] H. Ohno, D. Chiba, F. Matsukura, T. Omiya, E. Abe, T. Dietl, Y. Ohno, and K. Ohtani, Nature **408**, 944 (2000).

[7] D. Chiba, M. Yamanouchi, F. Matsukura, and H. Ohno, Science **301**, 943 (2003).

[8] P. Němec, E. Rozkotová, N. Tesařová, F. Trojánek, E. De Ranieri, K. Olejník, J. Zemen, V. Novák, M. Cukr, P. Malý, and T. Jungwirth, Nat. Phys. **8**, 411 (2012).

[9] N. Tesařová, P. Němec, E. Rozkotová, J. Zemen, T. Janda, D. Butkovičová, F. Trojánek, K. Olejník, V. Novák, P. Malý, and T. Jungwirth, Nat. Photon. **7**, 492 (2013).

[10] J. Zemen, J. Kučera, K. Olejník, and T. Jungwirth, Phys. Rev. B **80**, 155203 (2009).

[11] A. Dourlat, V. Jeudy, A. Lemaître, and C. Gourdon, Phys. Rev. B **78**, 161303(R) (2008).

[12] D. Chiba, M. Yamanouchi, F. Matsukura, T. Dietl, and H. Ohno, Phys. Rev. Lett. **96**, 096602 (2006).

[13] S. Haghgoo, M. Cubukcu, H. J. von Bardeleben, L. Thevenard, A. Lemaître, and C. Gourdon, Phys. Rev. B **82**, 041301(R) (2010).

[14] M. Yamanouchi, D. Chiba, F. Matsukura, T. Dietl, and H. Ohno, Phys. Rev. Lett. **96**, 096601 (2006).

[15] E. De Ranieri, P. E. Roy, D. Fang, E. K. Vehsthedt, A. C. Irvine, D. Heiss, A. Casiraghi, R. P. Campion, B. L. Gallagher, T. Jungwirth, and J. Wunderlich, Nat. Mater. **12**, 808 (2013).

[16] K. Y. Wang, A. W. Rushforth, V. A. Grant, R. P. Campion, K. W. Edmonds, C. R. Staddon, C. T. Foxon, B. L. Gallagher, J. Wunderlich, and D. A. Williams, J. Appl. Phys. **101**, 106101 (2007).

[17] A. Dourlat, V. Jeudy, C. Testelin, F. Bernardot, K. Khazen, C. Gourdon, L. Thevenard, L. Largeau, O. Mauguin, and A. Lemaître, J. Appl. Phys. **102**, 023913 (2007).

[18] D. Chiba, F. Matsukura, and H. Ohno, Appl. Phys. Lett. **89**, 162505 (2006).

[19] A. Lemaître, A. Miard, L. Travers, O. Mauguin, L. Largeau, C. Gourdon, V. Jeudy, M. Tran, and J.-M. George, Appl. Phys. Lett. **93**, 021123 (2008).

[20] A. W. Rushforth, M. Wang, N. R. S. Farley, R. P. Campion, K. W. Edmonds, C. R. Staddon, C. T. Foxon, and B. L. Gallagher, J. Appl. Phys. **104**, 073908 (2008).

[21] A. Casiraghi, A. W. Rushforth, M. Wang, N. R. S. Farley, P. Wadley, J. L. Hall, C. R. Staddon, K. W. Edmonds, R. P. Campion, C. T. Foxon, and B. L. Gallagher, Appl. Phys. Lett. **97**, 122504 (2010).

[22] M. Cubukcu, H. J. von Bardeleben, Kh. Khazen, J. L. Cantin, O. Mauguin, L. Largeau, and A. Lemaître, Phys. Rev. B **81**, 041202(R) (2010).

[23] A. Casiraghi, P. Walker, A. V. Akimov, K. W. Edmonds, A. W. Rushforth, E. De Ranieri, R. P. Campion, B. L. Gallagher, and A. J. Kent, Appl. Phys. Lett. **99**, 262503 (2011).

[24] L. Thevenard, S. A. Hussain, H. J. von Bardeleben, M. Bernard, A. Lemaître, and C. Gourdon, Phys. Rev. B **85**, 064419 (2012).

[25] P. Němec, V. Novák, N. Tesařová, E. Rozkotová, H. Reichlová, D. Butkovičová, F. Trojánek, K. Olejník, P. Malý, R. P. Campion, B. I. Gallagher, J. Sinova, and T. Jungwirth, Nat. Commun. **4**, 1422 (2013).

[26] C. Bihler, W. Schoch, W. Limmer, S. T. B. Goennenwein, and M. S. Brandt, Phys. Rev. B **79**, 045205 (2009).

[27] E. Rozkotová, P. Němec, P. Horodyská, D. Sprinzl, F. Trojánek, P. Malý, V. Novák, K. Olejník, M. Cukr, and T. Jungwirth, Appl. Phys. Lett. **92**, 122507 (2008).

[28] E. Rozkotová, P. Němec, N. Tesařová, P. Malý, V. Novák, K. Olejník, M. Cukr, and T. Jungwirth, Appl. Phys. Lett. **93**, 232505 (2008).

[29] An accurate determination of layer thicknesses is a nontrivial task in the case of thin (Ga,Mn)As layers [25]. Some standard techniques (e.g., x-ray reflectivity or optical ellipsometry) are inapplicable due to the weak contrast between the (Ga,Mn)As layer and the GaAs substrate or unknown optical parameters. The relative accuracy of other common techniques (e.g., of x-ray diffraction) does not exceed 10% because of the small thickness of the measured layer. Therefore, we used a thickness estimation based on the following quantities: (i) the growth time and the growth rate of the GaAs buffer layer measured by the reflection high-energy electron diffraction (RHEED) oscillations (typical accuracy of ±3%); (ii) increase in the growth rate by adding the known Mn flux measured by the beam-flux monitor relatively to the Ga flux (typical accuracy of ±5% of the Mn vs Ga flux ratio); (iii) reduction of thickness by the native oxidation (−1.5 nm ± 0.5 nm); (iv) reduction of thickness by thermal oxidation (−1.0 nm ± 0.5 nm). Relative accuracy of steps (i) and (ii) was verified on separate calibration growths of (Ga,Mn)As on AlAs, where an accurate x-ray reflectivity method to measure the (Ga,Mn)As layer thickness could be used. Typical thicknesses of the native and the thermal oxides in steps (iii) and (iv) were determined by x-ray photoelectron spectroscopy (XPS). The resulting total accuracy of the epilayer thickness determination is thus 3% (relative random error) and 1 nm (systematic error).

[30] M. Wang, K. W. Edmonds, B. L. Gallagher, A. W. Rushforth, O. Makarovsky, A. Patane, R. P. Campion, C. T. Foxon, V. Novak, and T. Jungwirth, Phys. Rev. B **87**, 121301 (2013).

[31] N. Tesařová, P. Němec, E. Rozkotová, J. Šubrt, H. Reichlová, D. Butkovičová, F. Trojánek, P. Malý, V. Novák, and T. Jungwirth, Appl. Phys. Lett. **100**, 102403 (2012).

[32] N. Tesařová, J. Šubrt, P. Malý, P. Němec, C. T. Ellis, A. Mukherjee, and J. Cerne, Rev. Sci. Intrum. **83**, 123108 (2012).

[33] N. Tesarova, T. Ostatnicky, V. Novak, K. Olejnik, J. Subrt, H. Reichlova, C. T. Ellis, A. Mukherjee, J. Lee, G. M. Sipahi, J.

Sinova, J. Hamrle, T. Jungwirth, P. Nemec, J. Cerne, and K. Vyborny, Phys. Rev. B **89**, 085203 (2014).
[34] N. Tesařová, E. Rozkotová, H. Reichlová, P. Malý, V. Novák, M. Cukr, T. Jungwirth, and P. Němec, J. Nanosc. Nanotechnol. **12**, 7477 (2012).
[35] Y. Hashimoto, S. Kobayashi, and H. Munekata, Phys. Rev. Lett. **100**, 067202 (2008).
[36] J. Qi, Y. Xu, A. Steigerwald, X. Liu, J. K. Furdyna, I. E. Perakis, and N. H. Tolk, Phys. Rev. B **79**, 085304 (2009).
[37] J. Miltat, G. Albuquerque, and A. Thiaville, in *Spin Dynamics in Confined Magnetic Structures I*, edited by B. Hillebrands and K. Ounadjela (Springer, Berlin, 2002), Chap. 1.
[38] M. van Kampen, C. Jozsa, J. T. Kohlhepp, P. LeClair, L. Lagae, W. J. M. de Jonge, and B. Koopmans, Phys. Rev. Lett. **88**, 227201 (2002).
[39] B. Lenk, G. Eilers, J. Hamrle, and M. Münzenberg, Phys. Rev. B **82**, 134443 (2010).
[40] X. Liu and J. K. Furdyna, J. Phys.: Condens. Matter **18**, R245 (2006).
[41] D. M. Wang, Y. H. Ren, X. Liu, J. K. Furdyna, M. Grimsditch, and R. Merlin, Superlatt. Microstruct. **41**, 372 (2007).
[42] M. Bombeck, A. S. Salasyuk, B. A. Glavin, A. V. Scherbakov, C. Bruggemann, D. R. Yakovlev, V. F. Sapega, X. Liu, J. K. Furdyna, A. V. Akimov, and M. Bayer, Phys. Rev. B **85**, 195324 (2012).
[43] X. Liu, Y. Y. Zhou, and J. K. Furdyna, Phys. Rev. B **75**, 195220 (2007).
[44] D. M. Wang, Y. H. Ren, X. Liu, J. K. Furdyna, M. Grimsditch, and R. Merlin, Phys. Rev. B **75**, 233308 (2007).
[45] A. Kalinikos and A. N. Slavin, J. Phys. C **19**, 7013 (1986).
[46] S. J. Potashnik, K. C. Ku, R. Mahendiran, S. H. Chun, R. F. Wang, N. Samarth, and P. Schiffer, Phys. Rev. B **66**, 012408 (2002).
[47] C. Gourdon, A. Dourlat, V. Jeudy, K. Khazen, H. J. von Bardeleben, L. Thevenard, and A. Lemaître, Phys. Rev. B **76**, 241301 (2007).
[48] T. G. Rappoport, P. Redlinski, X. Liu, G. Zaránd, J. K. Furdyna, and B. Jankó, Phys. Rev. B **69**, 125213 (2004).
[49] Y. Zhou, Y. Cho, Z. Ge, X. Liu, M. Dobrowolska, and J. K. Furdyna, IEEE T. Magn. **43**, 3019 (2007).
[50] A. Werpachovska and T. Dietl, Phys. Rev. B **82**, 085204 (2010).
[51] J. König, T. Jungwirth, and A. H. MacDonald, Phys. Rev. B **64**, 184423 (2001).
[52] S. Kobayashi, Y. Hashimoto, and H. Munekata, J. Appl. Phys. **105**, 07C519 (2009).
[53] J. Walowski, M. Djordjevic Kaufmann, B. Lenk, C. Hamann, J. McCord, and M. Munzenberg, J. Phys. D: Appl. Phys. **41**, 164016 (2008).
[54] Y. Liu, L. R. Shelford, V. V. Kruglyak, R. J. Hicken, Y. Sakuraba, M. Oogane, and Y. Ando, Phys. Rev. B **81**, 094402 (2010).
[55] A. A. Rzhevsky, B. B. Krichevtsov, D. E. Bürgler, and C. M. Schneider, Phys. Rev. B **75**, 224434 (2007).
[56] J. Walowski, G. Müller, M. Djordjevic, M. Münzenberg, M. Kläui, C. A. F. Vaz, and J. A. C. Bland, Phys. Rev. Lett. **101**, 237401 (2008).
[57] G. Woltersdorf, M. Buess, B. Heinrich, and C. H. Back, Phys. Rev. Lett. **95**, 037401 (2005).
[58] G. C Bailey and C. Vittoria, Phys. Rev. Lett. **28**, 100 (1972).
[59] J. Mašek, J. Kudrnovský, F. Máca, J. Sinova, A. H. MacDonald, R. P. Campion, B. L. Gallagher, and T. Jungwirth, Phys. Rev. B **75**, 045202 (2007).
[60] L. Thevenard, J.-Y. Duquesne, E. Peronne, H. J. von Bardeleben, H. Jaffres, S. Ruttala, J.-M. George, A. Lemaitre, and C. Gourdon, Phys. Rev. B **87**, 144402 (2013).
[61] A. G. Gurevich and G. A Melkov, *Magnetization Oscillations and Waves* (CRC Press, Boca Raton, Florida, 1996).